Analysis of the elastic and inelastic scattering of ^{32}S on ^{28}Si at energies from 77 to 135 MeV

A. Hemmdan[1*], Kassem O. Behairy[1], M. A. Hassanain[2], Norhan M. Nazem[1] and M. Anwar[1]

[1] Physics Department, Aswan University, Aswan 81528, Egypt

[2] Physics Department, New-Valley University, El-Kharga 72516, Egypt

Doi: 10.21608/nujbas.2023.242873.1013

Abstract

The elastic and inelastic differential cross-sections of ^{32}S on ^{28}Si at incident energies of 77, 90, 97.09, 120, and 135 MeV were analyzed. The first 2^+ excitation state in both nuclei as well as the [2^+, 2^+] mutual excitation were studied. The calculations were performed using double folding model. Three different potentials are used: the phenomenological Woods–Saxon double-folding cluster, in addition to the density-independent M3Y potential, which is considered for comparison. The imaginary potential part for the three potentials used was taken in the Woods-Saxon form. The influence of the inelastic channel on the elastic channel was investigated using the coupled channel method. Reasonable agreement for the considered experimental data for elastic and inelastic scattering was attained using the three generated potentials. The results of the cluster models show better agreement with the data than the other theoretical models. The total reaction and inelastic cross sections for low-lying excited states were extracted. The fitted deformation parameters for the transition potentials are also provided.

Keywords: Optical potential model; folding cluster model; M3Y-Reid interaction; Elastic and Inelastic scattering; coupled channels

1. INTRODUCTION

Heavy ion (HI) scattering at incident energies above the Coulomb barrier is considered a particularly important interaction for the determination of the ion-ion potential [1]. Therefore, the recent progress in experimental heavy ion physics has induced various theoretical investigations in this field [2–8]. In the case of ^{32}S, few high-resolution HI scattering measurements are available [9] as accurate measurements assimilate an interesting means of studying nuclear deformations when the shape of one of the colliding nuclei is well known.

In the past few decades, the double folding model has been successfully used to describe the elastic and inelastic scattering of two heavy ions [4]. The basic inputs in the folding calculation are the nuclear densities of the colliding nuclei and effective NN interaction. The simple density-independent M3Y interaction [10] has been widely used in various folding calculations of the HI potentials. It has been used with some success in folding model calculations of HI scattering [1], where the data are sensitive only to the potential at the surface in the vicinity of the strong absorption radius.

On the other hand, the α-cluster model successfully analyzed the elastic and inelastic scattering of various α-clustering nuclei [3,13–23]. The folding approach has been employed in the framework of the α-cluster model to extract a semi-microscopic description of the cluster potential with an α-α effective interaction [16]. In this context, the authors in [20, 21, 24, 25] and Karakoc and co-workers [17] have generated α-particle single folding cluster (SFC) and double folding cluster (DFC) optical potentials based upon an appropriate α-α effective interaction. They [17] assumed that the projectile and target nuclei consist of an integral multiple of α particles. However, in some of the studied reactions, it is essential to introduce a reducing description of the HI elastic scattering data. Yang and Li renormalization coefficients (~0.7–0.9) to obtain a successful [26] angular distribution calculations of ^{16}O + ^{16}O elastic scattering at incident energies that ranged from 75.0 to 350.0 MeV by using the α-folding potential.

EL-Azab Farid [27] also used the α- cluster structure for comparison with the M3Y potentials in the analysis of the ^{32}S+ ^{24}Mg reaction in the energy range of 65– 110 MeV. He noticed that the predictions of the derived DFC potential were in better agreement with the data at backward angles (better than in the rainbow angles) for the two highest energies than those of the M3Y DF potential. The same data for ^{32}S+ ^{24}Mg were measured and analyzed using the M3Y potentials by Pacheco et al. [28]. They obtained similar results using microscopic and semi-phenomenological potentials at the two lowest incident energies.

* Corresponding authors at: ahemdan@aswu.edu.eg

Various elastic and inelastic scattering experiments of HI for ^{32}S projectiles were accomplished at different incident energies near the Coulomb barrier [2, 9, 11, 12]. The main conclusion of these studies is that an accurate description of the experimental data claims the coupling with low-lying excited states.

In 1985, BAEZA et al. [29] studied the effect of different reaction mechanisms on the ^{32}S+^{28}Si interaction by measuring the elastic and inelastic cross sections at three sets of energies at 77.0, 90.0 and 97.09 MeV. They performed only a phenomenological analysis by fitting the elastic and first 2^+ states in each nucleus. They used two energy- independent optical potentials (T and A) for analysis. The study revealed that more realistic form factors computed from a microscopic model or a more realistic nuclear model are required to resolve the conflict between phenomenological calculations at low angles and the steepness of the slope at large angles for mutual excitation.

Bilwes and his collaborators [30] analyzed the elastic scattering data of ^{32}S on sd-nuclei (^{28}Si,^{32}S, ^{34}S, ^{40}Ca) over a large incident energy range. They attempted to overcome the phenomenological parameterization ambiguities in previous studies [9, 31]. They obtained a reasonable fit with the data by introducing a parity-dependent real part of the potential in their analysis to treat oscillations at backward angles. The calculated real and imaginary volume integrals of the studied ^{32}S+ ^{28}Si system did not indicate the dispersion relation.

The experimental data for the elastic and inelastic scattering of ^{32}S+ ^{28}Si were only partially studied in [9]. The precise experimental data of mutual excitation of the two deformed s-d (^{32}S-^{28}Si) nuclei have been measured at the first 2^+ excitations in both nuclei at 90.0 and 97.09 MeV [31] . The same data for the elastic, inelastic quadrupole (2^+), octupole (3^-) and mutual (2^+,2^+) excitation cross sections have been measured at 77.0, 90.0 and 97.09 MeV over a wide angular range [9]. Single and mutual excitation analyses are only performed phenomenologically using the coupled channel (CC) method. The form factors for single and mutual excitations were generated by deforming the real, imaginary, and Coulomb parts of the potential. They showed a remarkable sensitivity to the sign of the deformation and the nuclear component was sufficient to provide almost the total nuclear shape for mutual excitation. They also suggested that using microscopic form factors may improve the agreement of the theoretical calculations with the experimental data; however, the additional coupling to the mutual excitation worsens the fit and displaces the position of the minima of the 2^+ level curves.

From the previous studies, few theoretical analyses have been presented in the literature regarding the ^{32}S+^{28}Si scattering [9,31–33]. Conventional OM analysis fails to reproduce all or some of the experimental data [9,32]. In addition, there have been no detailed microscopic studies using folding models that attempt to explain angular distributions. The analysis of the elastic and inelastic scattering of ^{32}S on the sd-nuclei near the Coulomb barrier requires further theoretical efforts. Moreover, the influence of one excitation of the colliding nuclei or mutual excitation on the elastic channel and oscillations at backward angles also require further investigation.

Therefore, the main objective of the present work is to reanalyze elastic and inelastic ^{32}S+^{28}Si scattering at an energy range of 77-135 MeV using the double folding cluster (DFC) potential. The results are shown in comparison with the double folding M3Y-Reid NN interaction potential and phenomenological Woods-Saxon (WS) potential. Inelastic scattering, the first 2^+ excitation of both ^{32}S and ^{28}Si nuclei, and their mutual [2^+,2^+] excitation were studied using CC calculations at 77.0, 90.0 and 97.09 MeV incident energies.

This work is organized as follows: A brief description of the derived formalisms and the procedures are given in Sec. II and III, respectively. Section IV is devoted to the results and discussion. Finally, conclusions are reported in Sec. V.

2. THEORITICAL FORMALISM

1.2 Elastic scattering

In the present work, we analyzed the elastic scattering of ^{32}S+^{28}Si at various energies of 77.0, 90.0, 97.09, 120 and 135 MeV. Calculations were performed based on the optical model potential (OP) using double folding M3Y (DFM) and double folding cluster (DFC) potentials. The total nuclear potential can be represented by the real part v (r) and imaginary potential part w (r) as follows:

$$\mathrm{U(r)} = \mathrm{V(r)} + \mathrm{iW(r)} \quad (1)$$

Heavy ions scattering is characterized by strong absorption, which makes the data sensitive only to the surface part of the nucleus- nucleus potential then eq.(1) can be written as follows [34]:

$$\mathrm{V(r)} = \mathrm{V_C(r)} + \mathrm{V(r)} + \mathrm{w(r)} \quad (2)$$

Where, the Coulomb potential $V_C(R)$ is taken as a uniformly charged sphere of radius $R_C = 1.2\ (A_T^{1/3} + A_P^{1/3})$. A_T and A_P are the masses of target and projectile, respectively.

In this study, the optical potential was calculated in three forms. In the first form, the phenomenological WS is used to calculate the nuclear potential:

$$\mathrm{V(r)} = V_0\ \mathrm{fv(r)(r)} - \mathrm{i}W_0\mathrm{f_w(r)} \quad (3)$$

$$f_x(r) = [1 + \exp\left(\frac{r - r_x\left(A_P^{1/3} + A_T^{1/3}\right)}{a_x}\right)^{-1}, x = v, w \quad (4)$$

The parameters, $V_0(W_0)$, $R_V(R_W)$ and $a_V(a_W)$ are the depth, radius and diffuseness of the real (imaginary) potential, respectively.

At low-energies scattering, optical model potential suffers from discrete and continuous ambiguities, whose uncertainties vary for various target nuclei and for different incident energies owing to the precision of the data analyzed. Therefore, to avoid phenomenology in the description of these data, numerous attempts have been made to replace the phenomenological real potential of the WS type by a semi microscopic potential based on a suitable effective nucleon-nucleon interaction.

The second form of the real nuclear potential is calculated using the double folding potential [1] as the following:

$$V_{DF}(R) = N_R \iint \rho_1(\mathbf{r}_1)\rho_2(\mathbf{r}_2)\, v_{nn}(\boldsymbol{s}) d\mathbf{r}_1 d\mathbf{r}_2,\ \boldsymbol{s} = \mathbf{R} - \mathbf{r}_1 + \mathbf{r}_2 \quad (5)$$

N_R, is the real normalization factor, $\rho_1(r_1)$ and $\rho_2(r_2)$ are the density of projectile and target respectively while $v_{NN}(s)$ is the nucleon- nucleon interaction potential.

In the present work, we used 3Fp density form [35] for both projectile and target nucleus that is given by:

$$\rho(r) = \rho_o(1 + w(\frac{r}{z})^2)(1 + \exp(\frac{r-z}{\beta}))^{-1}\ \text{Fm}^{-3} \quad (6)$$

With the matter density parameters, z and β are given in table (1). The parameters are taken from [36].

The NN interaction is taken as M3Y effective interaction [1] as follows:

$$v_{nn}(s) = 7999\frac{\exp(4s)}{4s} - 2134\frac{\exp(2.5s)}{2.5s} + J_{oo}(E)\delta\ \text{MeV} \quad (7)$$

Where, δ(r) term accounts for knock exchange and $J_{oo}(E)$ is a linearly energy-dependent strength in the form:

$$J_{oo}(E) \approx -276\left[1 - {}^{0.005E}/_{A_P}\right]\ \text{MeV Fm}^{-3} \quad (8)$$

The imaginary part of the calculated nuclear potentials is taken as Wood Saxon form as given in eq. (3). The OPM in the semi-microscopic case is considered to be more acceptable physically than phenomenological one since it contains the basic physical ingredients the nuclear density folded with a realistic nuclear interaction in the correct way [37]. The third form of the real nuclear potential based upon the α-cluster structure, ^{32}S as (8α) and ^{28}Si as (7α) constructed. is calculated as [3]:

$$V_{DFC}(R) = (N_R)\int\int \rho_{C_1}(r_1)\rho_{C_2}(r_2)v_{\alpha\alpha}(\mathbf{s})d\mathbf{r_1}\, d\mathbf{r_2}. \quad (9)$$

Where, $v_{\alpha\alpha} = -122.6226\exp(-22s^2)$

In this case, both colliding nuclei are considered as α -clusters therefore α-α effective interaction folded with α -clusters distribution densities, $\rho_C(r)$ for projectile. where, ρ_{C_1} and $\rho_{C_2}(r_2)$ are the cluster densities of the ^{32}S and ^{28}Si respectively and given by [34, 38, 39]:

$$\rho_C(r') = \rho_0^c\left(1 + \gamma^c\left(\frac{r'}{Z^c}\right)^2\right)\left[1 + exp\left(\frac{r'-Z^c}{\alpha^c}\right)\right]^{-1} \quad \text{fm}^{-3} \quad (10)$$

The parameters $\boldsymbol{\omega^c}$, Z^c and then β^c of the ^{32}S and ^{28}Si α-cluster densities are taken as in ref. [38] and given in Table (1). by postulating a form of potential and adjusting its parameters to optimize the fit to the experimental data by minimizing the chi-square χ^2.

$$\chi^2 = \frac{1}{N}\sum_{i=1}^{N}\left[\frac{\sigma_{th}(\theta_i) - \sigma_{exp}(\theta_i)}{\Delta\sigma_{exp}(\theta_i)}\right]^2 \quad (11)$$

Where, $\sigma_{th}(\theta_i)$ and $\sigma_{exp}(\theta_i)$ are the theoretical and experimental differential cross sections, respectively at an angle θ_i, N is the number of angles at which measurements are done and $\Delta\sigma_{exp}(\theta_i)$ is the error associated with $\sigma_{exp}(\theta_i)$.

Table 1. The 3pF matter (cluster) densities parameters and rms for the ^{32}S, ^{28}Si and ^{16}O:

Nucleus	$\omega(\gamma^C)$	$z(z^C)$ [fm]	β (α^C) [fm]	rms [fm]
^{32}S	-0.213(0.234)	3.441(3.137)	0.624(0.274)	3.24(2.87)
^{28}Si	-0.149(0.230)	3.239(3.055)	0.574(0.259)	3.13(2.77)

2.2 Inelastic scattering

The phenomenological WS and the two OPs based upon DFC and M3Y are used to perform the calculations of the inelastic ^{32}S + ^{28}Si scattering cross sections at three energy values 77.0, 90.0 and 97.09 MeV, for the low-lying 2^+ state ($E_{ex.} = 1.78$ MeV) of the target ^{28}Si nucleus, 2^+ state ($E_{ex.} = 2.23$ MeV) of the projectile ^{32}S nucleus and the mutual excitation for the colliding nuclei ^{32}S $_{2.23}(2^+)$ and ^{28}Si$_{1.78}(2^+)$ by using CC approach.

Firstly, the deformed potential (DP) is obtained by the derivative of the WS potential for the multi-polarity λ . In this case, the DP whose shape is independent of λ is given by [40].

$$U_{\lambda}^{\mathrm{WS}}(R) = -\frac{\delta_{\lambda}}{\sqrt{4\pi}} dU(R)/dR, \quad (12)$$

The generated real nuclear transition potential DFC (M3Y) can be calculated in terms of the transition density for the target or projectile or both of them with the effective interaction as follows:

$$U_{\lambda}^{tr} = N_R \iint \rho_P^{\lambda 0(2)}(\boldsymbol{r_1})\, \rho_T^{\lambda 0(2)}(\boldsymbol{r_2})\, v_{nn(\alpha\alpha)}(\boldsymbol{s}) d\boldsymbol{r_1} d\boldsymbol{r_2}, \quad (13)$$

Where $\lambda 0(2)$ represents the ground 0^+ (2^+) state and $\rho_P^{\lambda 0(2)}(\boldsymbol{r_1})\, \rho_T^{\lambda 0(2)}(\boldsymbol{r_2})$ refers to $\rho_P^{\lambda 0}(\boldsymbol{r_1})\, \rho_T^{tr}(\boldsymbol{r_2})$, $\rho_P^{tr}(\boldsymbol{r_1})\, \rho_T^{\lambda 0}(\boldsymbol{r_2})$and $\rho_P^{tr}(\boldsymbol{r_1})\, \rho_T^{tr}(\boldsymbol{r_2})$ for the single 2^+ excitation of target, projectile and mutual excitation respectively. The $\rho_{\lambda(i)}^{tr}(r)$ is the transition density that derived according to,

$$\rho_{(i)}^{tr}(r) = \delta_2^{m(c)}\, d\rho_i/dr, \quad (14)$$

since, $\rho_i(r)$ is the ground state density distribution of the projectile ^{32}S nucleus or the target ^{28}Si nucleus. $\delta_2^{m(c)}$ represents the matter (cluster) deformation length which provides a measure of the nuclear transition rate. It is given by

$$\delta_2^{m(c)} = \beta_2 R \quad (15)$$

Where, β_2 is the deformation parameter and R is the radius of the deformed nucleus ($R = 1.2\, A^{1/3}\, fm$). The deformation parameter relates to the measured $\beta(E\lambda)$ transition rate by $\beta_{\lambda} = \frac{4\pi}{3ZR^2}[B(E\lambda; I \to I')b^2e^2/e^2]^{1/2}$. Coulomb deformations of nuclei were introduced in terms of reduced transition probabilities. $B(E2; 0^+ \to 2^+)$ = 0.02914 e^2b^2 for ^{32}S and $B(E2; 0^+ \to 2^+)$ = 0.03281 e^2b^2 for ^{28}Si are obtained from Ref. [41] and were used to describe Coulomb deformations of both projectile and target. According to Ref. [1] , the equal deformation hypothesis for matter distribution and potential is, in fact, correct if the projectile is a point-like particle and the potential is obtained by folding the density with a zero range interaction. The correct deformation length (δ_{λ}^{corr}) is adopted for the deformed potential as in Refs. [18, 42] to take into account the relative differences in the density and potential radii, as follows:

$$\delta_{\lambda}^{corr} = \delta_{\lambda}\, R/R_{pot} \quad (16)$$

R_{pot}, is the radius of the considered potentials. For M3Y (DFC), R_{pot} = 4.03 fm (4.026 fm). In our calculations, we assume that the imaginary deformation length is equal to the matter deformation. Therefore, the corrected deformation lengths for ^{32}S are 1.1 fm and 1.35 fm for ^{28}Si. For the imaginary transition potential, the derivative of the imaginary central potential is obtained from,

$$W_{\lambda}^{WS}(R) = -\frac{1}{\sqrt{4\pi}} \delta_2^{\mathrm{w}}\, dW(R)/dR, \quad (17)$$

Where, δ_2^wrefers to the imaginary deformation length defined as: $\delta_2^w = \beta_2^W R_W$, , and β_2^W is the imaginary deformation parameter.

The generated three real optical potentials at the energy 97.09 MeV are shown in Fig. 1. The potentials have the same strength and slope at the surface, i.e., at the small overlap or low-density region. The slightly difference between the obtained semi-microscopic potentials DFC and M3Y is shown at short inter-nuclear distance, which corresponds to the higher overlap density of the colliding nuclei. In contrast, the real WS potential is of shallow depth. The general trend of the real volume part depth shows clear energy dependence as it increases with increasing energy as demonstrated in Table 2. Also, a random behavior for the weak depth of the volume imaginary part is noticed.

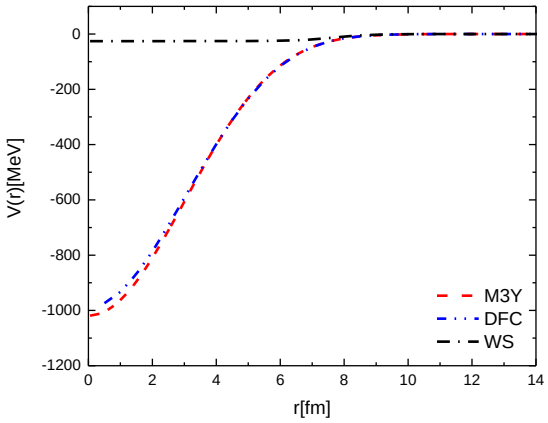

Fig. 1. The generated three real potentials for ^{32}S + ^{28}Si elastic scattering, DFC (blue double dot) in comparison to M3Y (red dashed) and WS (black dash dot).

Table 2. The best fit parameters of the OPs, WS, M3Y and DFC that obtained for the elastic $^{32}S + ^{28}Si$ scattering.

E (MeV)	Potential	N_R	V (MeV)	r_R (fm)	a_R (fm)	$-J_R$ (MeV fm^{-3})	W (MeV)	rI (fm)	aI (fm)	$-J_I$ (MeV fm^{-3})	σ_R (mb)	χ^2
	WS		17.3	1.384	0.495	52.86	2.352	1.604	0.108	10.89	417.4	0.69
77.0	M3Y	1.0				419.4	2.82	1.585	0.131	12.61	405.2	0.71
	DFC	1.0				427.2	2.65	1.63	0.108	12.38	439.8	0.71
	WS		36.2	1.3	0.425	94.39	2.265	1.0	1.488	4.026	813.0	4.78
90.0	M3Y	0.77				326.1	2.266	1.59	0.25	12.23	879.8	6.2
	DFC	1.04				444.2	2.42	1.6	0.267	12.28	861.1	5.47
	WS		41.15	1.255	0.497	94.78	2.95	0.93	1.322	4.022	848.1	10.0
97.09	M3Y	0.73				304.8	3.875	1.43	0.435	13.0	873.3	13.0
	DFC	0.8				330.8	4.40	1.321	0.587	11.94	839.1	11.2
	WS		76.64	1.06	0.66	111.9	2.023	1.59	0.415	9.269	1392	2.4
120.0	M3Y	0.8				333.2	4.2	1.38	0.446	12.70	1185	3.1
	DFC	0.9				377.2	5.153	1.327	0.532	14.04	1197	2.6
	WS		176.88	1.076	0.684	272.4	5.28	1.39	0.606	38.32	1542	0.33
135.0	M3Y	0.778				323.5	8.96	1.33	0.573	24.64	1486	0.451
	DFC	0.878				363.0	10.63	1.28	0.665	26.39	1522	0.332

3. Procedure

The elastic scattering for the reactions of $^{32}S+^{28}Si$ at five sets of energies (77.0, 90.0, 97.09, 120.0 and 135.0 MeV) has been analyzed with three nuclear potential forms; two semi-microscopic potentials (DFC and M3Y) and the third is the phenomenological WS. The calculations are performed using the following procedures:

1. The complex phenomenological potential (WS) used Eq. (3) and the two semi-microscopic potentials (M3Y and DFC) with (Eq. (5) and (9)) for the elastic $^{32}S+^{28}Si$ scattering

2. The program codes HERMIZ [43] and FRESCO [44] program are executed using the automatic search option to calculate the elastic scattering differential cross sections of the considered experimental data. The quality of agreement with data can be arbitrated by χ^2scale. The calculations are achieved for the considered data with the experimental errors of 10% as an average value.

3. The search was carried out on six parameters of WS (three parameters for real volume part and three of imaginary one) while, the search in the two mentioned semi-microscopic potentials cases (DFC and M3Y) was attained by four parameters of: (Normalization coefficient and the three parameters of the WS volume imaginary part) in the elastic scattering case.

4. The calculations of the inelastic $^{32}S+^{28}Si$ scattering fit are obtained through the automatic search option in FRESCO code [44] in the framework of the CC mechanism at low-lying excited states for projectile and target. It can be categorized as follows:

A) Channel 1: elastic channel: $^{32}S_{gs} + ^{28}Si_{gs}$

B) Channel 2: single-excitation channel of $^{32}S_{2.23} + ^{28}Si_{gs}$

C) Channel 3: single-excitation channel of $^{32}S_{gs} + ^{28}Si_{1.78}$

D) Channel 4: mutual-excitation channel of $^{32}S_{2.23} + ^{28}Si_{1.78}$

Then, the types of calculations are categorized as,

a) Single-channel calculation that includes only the elastic channel A)

b) CC calculation with single excitation with Channel A) + B)

c) CC calculation with single excitation with Channel A) + C)

d) CC calculation with single excitations with Channel A) + B) + C)

e) CC calculation with single and mutual excitations with Channel A) + B) + C) + D)

In the inelastic case, we used the same WS parameters and searched for the deformation and normalization parameters.

4. Results and discussion

In the present work, the differential cross section of $^{32}S + ^{28}Si$ elastic and inelastic scattering in energies around the Coulomb barrier at five sets of data, E_{lab}=77.0, 90, 97.09, 120, and 135.0 MeV are analyzed. The

elastic and inelastic cross sections are calculated by using three considered WS, DFC and M3Y potentials. The obtained best fit parameters of the elastic scattering part are listed in Table 2 and Table 3 for the inelastic parameters.

Table 3: The $^{32}S+^{28}Si$ inelastic scattering normalization factor and deformation parameters that fitted for the M3Y and DFC potentials.

E (MeV)	Potential	N_R	β_2 (Si)	β_2 (S)
77.0	M3Y	1.0	-0.33	-0.20
	DFC	1.0	-0.36	-0.23
90.0	M3Y	1.0	0.3	0.289
	DFC	1.04	0.37	-0.315
97.09	M3Y	0.96	0.4	0.2415
	DFC	1.0	0.37	0.289

The $^{32}S + ^{28}Si$ elastic scattering:

The results of the calculated cross section are displayed in Fig. 2. The angular differential cross sections for the elastic scattering data sets 77.0, 90.0, 97.09, 120.0, and 135.0 MeV under study, are reproduced by using WS potential as shown in Fig. 2. It is obvious that the present calculated angular distribution exhibits a good agreement with the experimental data. At the first three energies 77.0, 90.0, 97.09 MeV, our calculations reveal better agreement than those presented in Ref. [10, 22]. This successful fitting with data is apparent for all the extracted new parameters in comparison with the previous phenomenological analysis given in Refs [10, 22]. For the microscopic analysis as shown in Fig. 3, successful results were reproduced for all the studied energies using the two semi-microscopic DFC and M3Y potentials. Both potentials produce almost identical predictions and comparable values for the parameters using a reduction factor of the generated potentials. Despite this successfully reproduced the data, unreasonable agreement is found for 97.09 MeV at the backward angles. The most probably cause of this disagreement is the transfer processes of α-alpha particle [32]. Cluster and nucleon exchange effects have indeed been observed to be dominate at large angle elastic scattering in a number of nuclear systems [45].

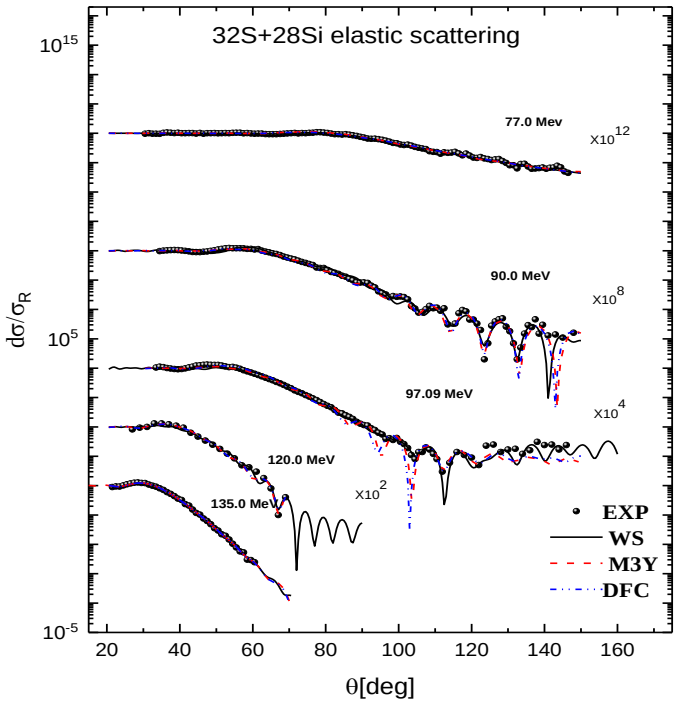

Fig. 2 The experimental elastic angular distribution for $^{32}S+^{28}Si$ scattering at the energies 77.0, 90.0, 97.09, 120 and 135 MeV in comparison to the theoretical predictions of the optical WS (solid line), M3Y (dash line), and DFC (dash double dot line). The experimental data are taken from refs [9, 32].

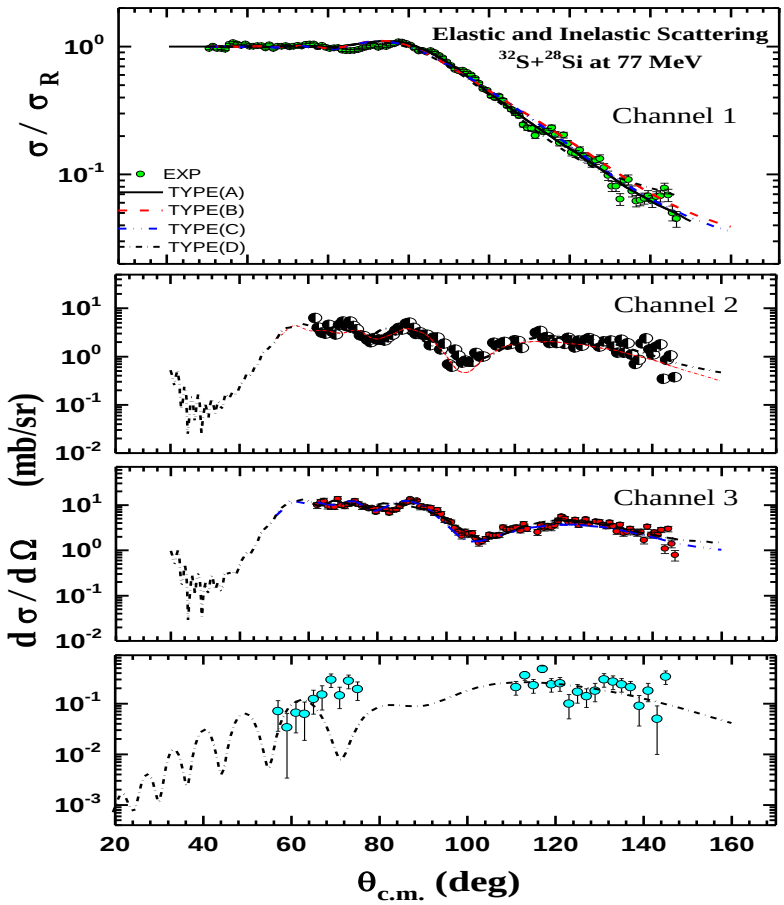

Fig. 3. The experimental angular distributions for the low-lying 2+ state of ^{32}S projectile and 2^+ state of ^{28}Si target and the mutual excitation of both projectile and target ($2^+ \cdot 2^+$) populated in the ^{32}S+^{28}Si inelastic scattering at 77 MeV in comparison to the predictions of WS potential. The effect of CC calculations on the elastic channels is shown in the top panel. Experimental data are taken from [9].

The ^{32}S + ^{28}Si inelastic scattering:

Inelastic scattering process is one of the most processes that take place when two heavy ions collide, and gained via the excitation of low-lying collective modes at energies close to coulomb barrier and powerful interactions, the importance of this process expressed in the combination of inelastic excitation with a transfer process in addition to the ability of gaining information over the nuclear surface interactions and deformations. For these reasons we have analyzed the high- resolution measurements of both inelastic scattering of ^{32}S on ^{28}Si at 77.0, 90.0 and 97.09 MeV.

As a starting point, we used the same optical potentials WS, M3Y and DFC parameters that are fitted to the elastic cross section and searched for the deformation parameters. Figs. 3 to 11 show the coupled channel calculations of the cross sections for the elastic, 2^+ excitation, in addition to the mutual excitation. The calculations were done for four channels with the transition potentials of M3Y and DFC as well as the deformed WS potential cross sections at the three energies 77.0, 90.0 and 97.09 MeV.

In order to improve the agreement with data, we adjusted the optical parameters by fitting elastic and 2^+ inelastic curves in two channel calculations for each nucleus separately to notice the difference in coupling strengths, which show a good agreement with experimental data for the mentioned potentials except for the back word angles of 97.09 which show unsatisfactory agreement at the back angles, as a result of the transfer process of α- alpha particle. The additional coupling to the mutual excitation worsens the fit and displaced the position of the minima of the 2^+ level curves for 90.0 and 97.09 MeV expected for 77.0 MeV which has an upgrade fitting. Very satisfactory reproductions of the inelastic and the corresponding elastic data are obtained from all considered potentials. Including the CC effect improved the normalization factor in case of DFC potential model compared to M3Y potential while the effect of the CC to the fitting of elastic data is found to be tiny.

5. Conclusion

The differential cross sections of elastic and inelastic scattering for the ^{32}S + ^{28}Si system at the energies 77.0, 90.0, 97.09, 120.0, and 135.0 MeV have been performed in the framework of nuclear optical model. A successful

description of the considered experimental data for elastic and inelastic scattering has been presented using the traditional WS phenomenological potential in addition to DFC and M3Y semi-microscopic OPs. The imaginary part of the two derived potentials is used as a phenomenological WS form. The theoretical angular distribution calculations give better agreement with experimental data in four channels, 0^+, ${}^{28}_{1.78}Si(2^+)$, ${}^{32}_{2.23}S(2^+)$ and $(2^+, 2^+)$ than the previous phenomenological analysis in Ref. [9]. Moreover, both M3Y and DFC potentials model improved the value of N_r to be close one ($N_r = 1.0 \pm 0.1$). DFC results show better agreement with data in comparison to the WS and M3Y potentials. Indeed, the effect of the coupling of the form factors for the mutual excitation and the single inelastic excitation on the elastic channel is found to be tiny.

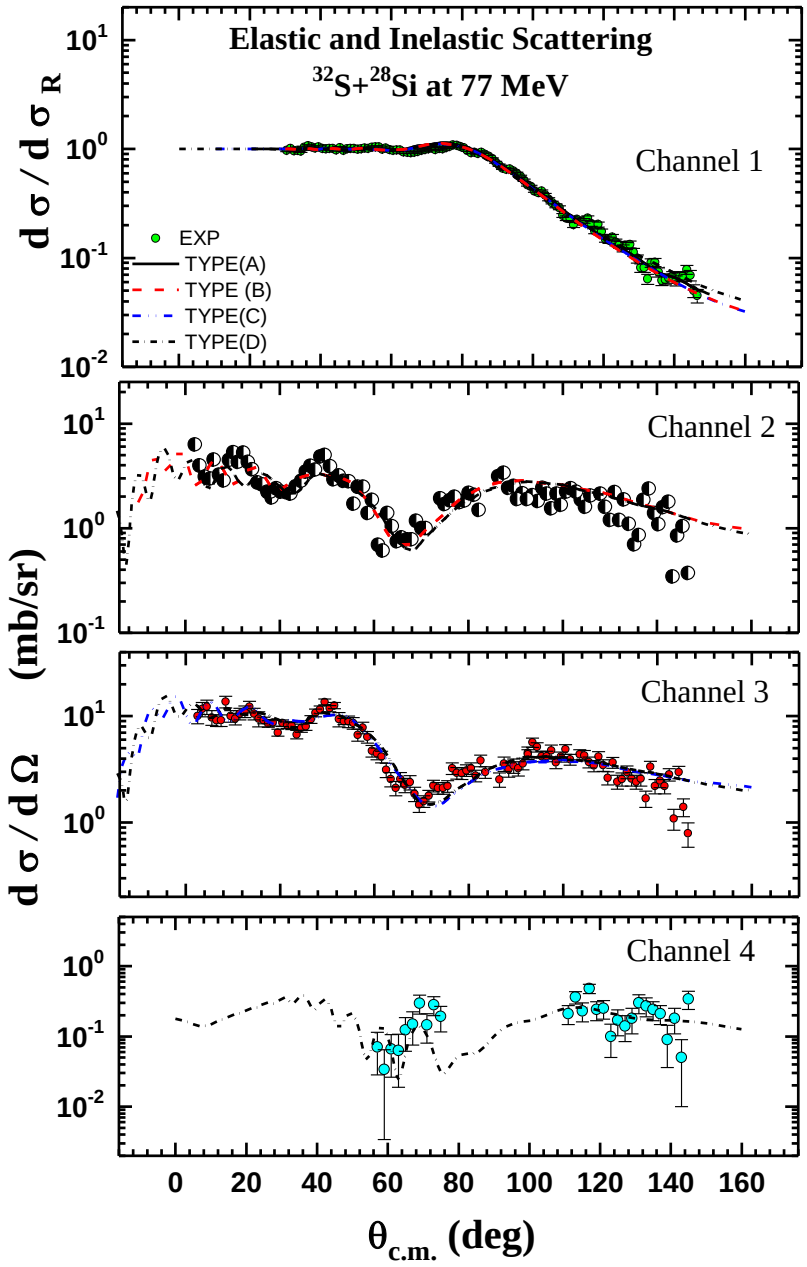

Fig. 4. The same as Fig. 3 but for M3Y potential.

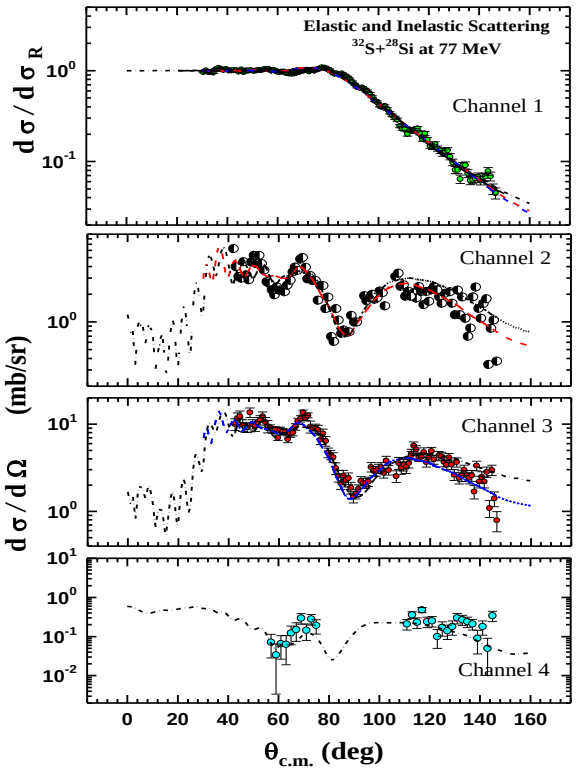

Fig. 5. The same as Fig. 3 but for DFC potential.

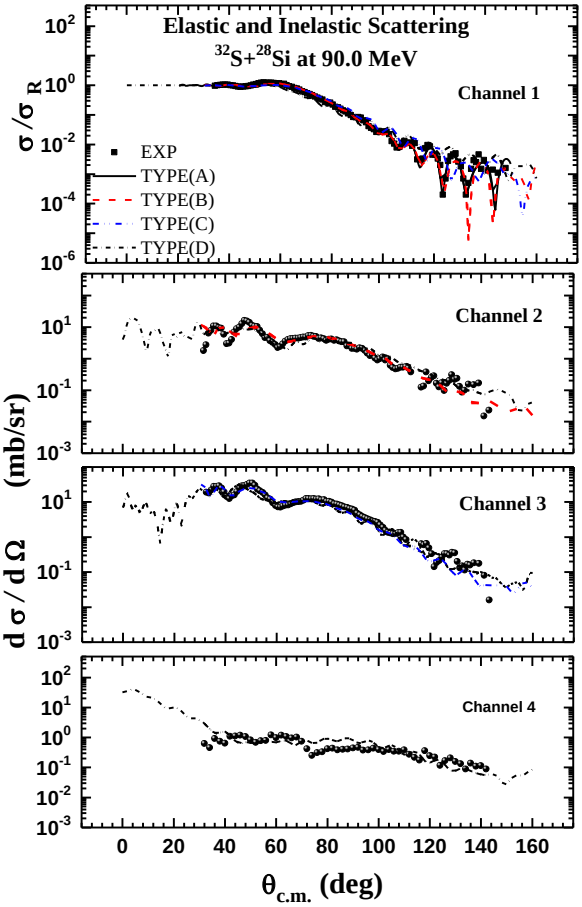

Fig. 6. The experimental angular distributions for the low-lying 2+ state of ^{32}S projectile and 2^+ state of ^{28}Si target and the mutual excitation of both projectile and target (2^+ 2^+) populated in the ^{32}S+^{28}Si inelastic scattering at 90.0 MeV in comparison to the predictions of WS potential. The effect of CC calculations on the elastic channels is shown in the top panel. Experimental data are taken from [9].

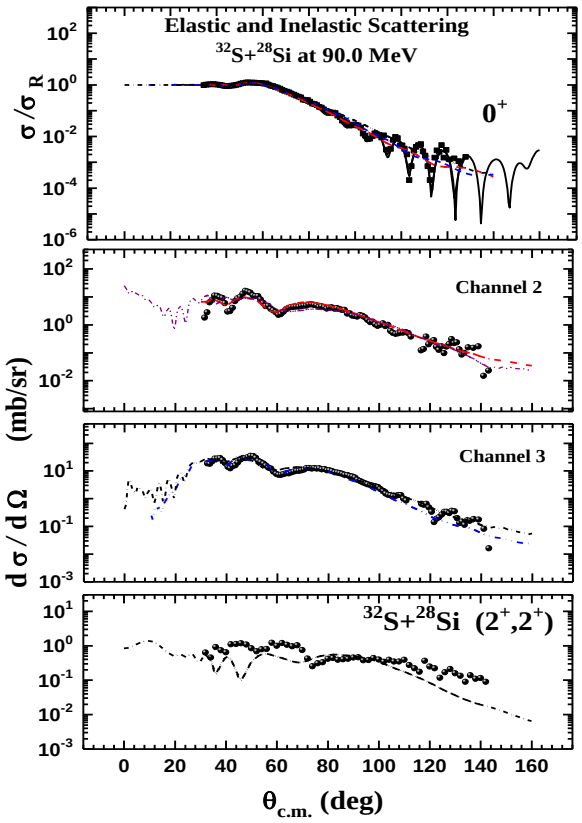

Fig. 7. The same as Fig. 6 but for M3Y potential.

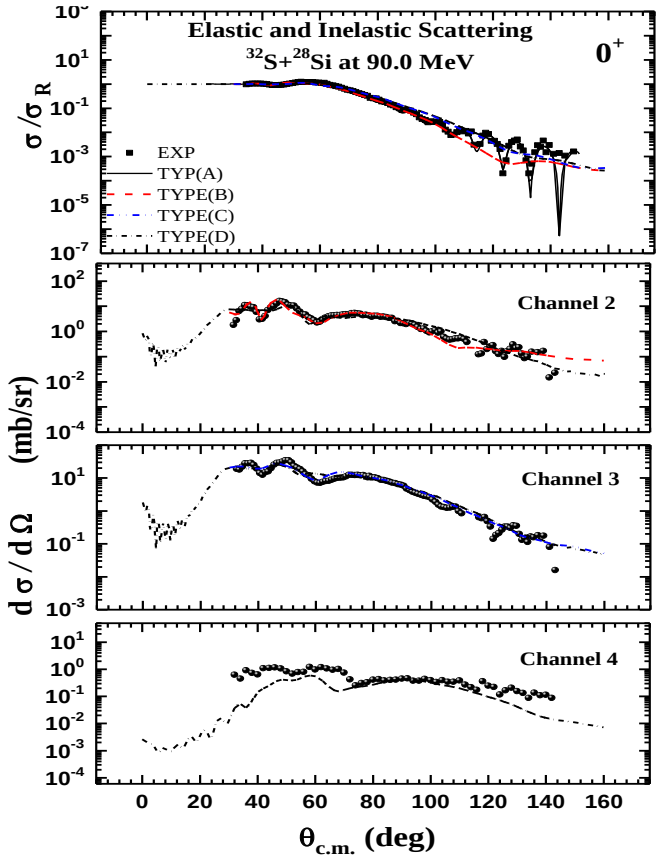

Fig. 8. The same as Fig. 6 but for DFC potential.

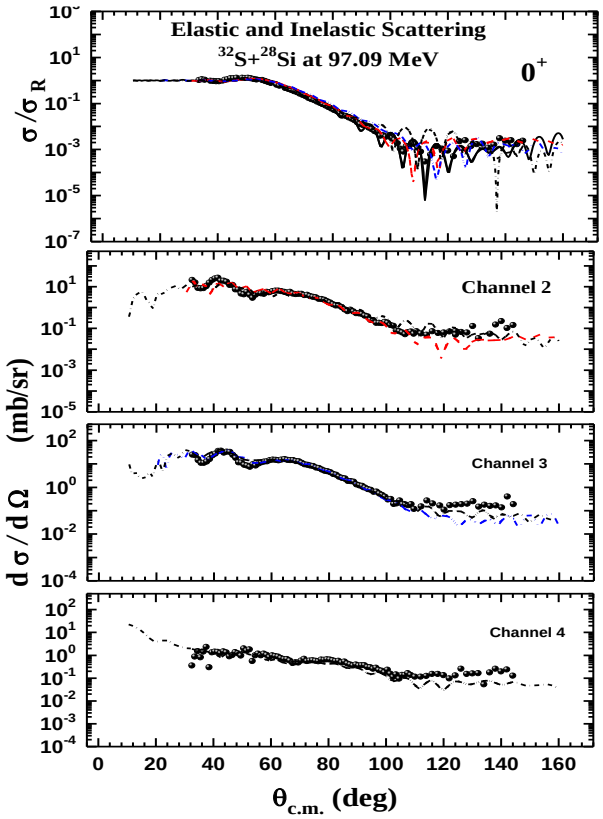

Fig. 9. The experimental angular distributions for the low-lying 2+ state of ^{32}S projectile and 2^+ state of ^{28}Si target and the mutual excitation of both projectile and target (2^+2^+) populated in the ^{32}S+^{28}Si inelastic scattering at 97.09 MeV in comparison to the predictions of WS potential. The effect of CC calculations on the elastic channels is shown in the top panel. Experimental data are taken from [9].

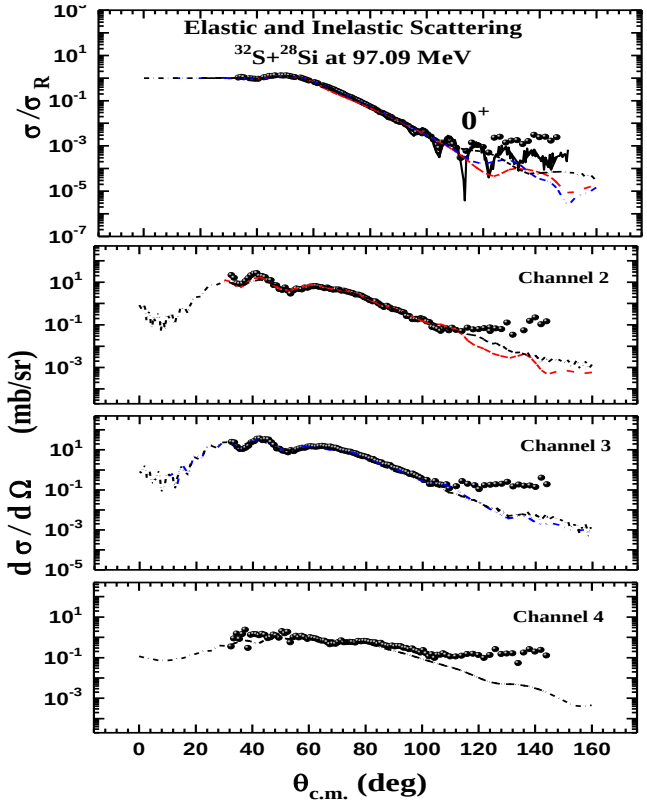

Fig. 10. The same as Fig. 9 but for M3Y potential.

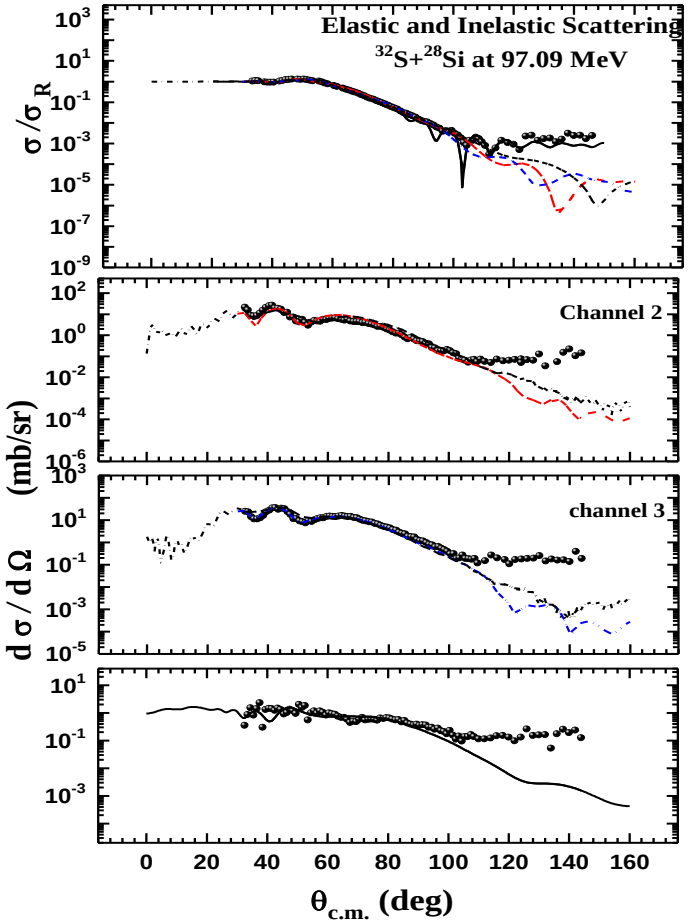

Fig. 11. The same as Fig. 9 but for DFC potential.

References

[1] - G. R. Satchler and W. G. Love, Phys. Rep. **55**, 183 (1979).

[2] - G. R. Satchler, Phys. Rep. **199**, 147 (1991).

[3] - M. E.-A. Farid, Z. M. M. Mahmoud, and G. S. Hassan, Nucl. Phys. A **691**, 671 (2001).

[4] - M. A. Hassanain and A. A. Ibraheem, Brazilian J. Phys. **45**, 699 (2015).

[5] - F. Cappuzzello, D. Nicolosi, R. Linares, J. R. B. Oliveira, J. Lubian, C. Agodi, D. Carbone, M. Cavallaro, P. N. de Faria, A. Foti, and M. R. D. Rodrigues, Eur. Phys. J. A **52**, (2016).

[6] - V. A. B. Zagatto, F. Cappuzzello, J. Lubian, M. Cavallaro, R. Linares, D. Carbone, C. Agodi, A. Foti, S. Tudisco, J. S. Wang, J. R. B. Oliveira, and M. S. Hussein, Phys. Rev. C **97**, 1 (2018).

[7] - L. M. Fonseca, R. Linares, V. A. B. Zagatto, F. Cappuzzello, D. Carbone, M. Cavallaro, C. Agodi, J. Lubian, and J. R. B. Oliveira, Phys. Rev. C **100**, 1 (2019).

[8] - T. Ulucay and M. Aygun, Rev. Mex. Fis. **66**, 336 (2020).

[9] - A. Baeza, B. Bilwes, R. Bilwes, J. Diaz, J. L. Ferrero, and J. Raynal, Nucl. Phys. A **437**, 93 (1985).

[10] - G. Bertsch, J. Borysowicz, H. McManus, and W. G. Love, Nucl. Phys. A **284**, 399 (1977).

[11] - M. Richter, W. Henning, H.-J. Körner, R. Müller, K. E. Rehm, H. P. Rother, H. Schaller, and H. Spieler, Nucl. Phys. A **278**, 163 (1977).

[12] - J. Díaz, J. L. Ferrero, J. A. Ruiz, B. Bilwes, R. Bilwes, J. Diaz, J. L. Ferrero, J. A. Ruiz, B. Bilwes, and R. Bilwes, Nucl. Phys. A **494**, 311 (1989).

[13] - M. El-Azab Farid, Z. M. M. Mahmoud, and G. S. Hassan, Phys. Rev. C - Nucl. Phys. **64**, 143101 (2001).

[14] - M. E.-A. Farid, A. A. Ibraheem, J. H. Al-Zahrani, W. R. Al-Harbi, and M. A. Hassanain, J. Phys. G Nucl. Part. Phys. **40**, 75108 (2013).

[15] - Z. M. M. Mahmoud, A. A. Ibraheem, and M. E. A. Farid, J. Phys. Soc. Japan **81**, 1 (2012).

[16] - M. El-Azab Farid, Phys. Rev. C **65**, 67303 (2002).

[17] - M. Karakoc and I. Boztosun, Phys. Rev. C **73**, 47601 (2006).

[18] - A. Hemmdan, M. A. Hassanain, M. Anwar, and K. O. Behairy, Phys. Rev. C **104**, 1 (2021).

[19] - Y.-X. Yang and Q.-R. Li, Phys. Rev. C **84**, 14602 (2011).

[20] - M. A. Hassanain, A. A. Ibraheem, and M. E.-A. Farid, Phys. Rev. C **77**, 34601 (2008).

[21] - M. A. Hassanain, A. A. Ibraheem, S. M. M. Al Sebiey, S. R. Mokhtar, M. A. Zaki, Z. M. M. Mahmoud, K. O. Behairy, and M. E. A. Farid, Phys. Rev. C - Nucl. Phys. **87**, (2013).

[22] - D. M. Brink and J. J. Castro, Nucl. Phys. A **216**, 109 (1973).

[23] - A. H. Al-Ghamdi, A. A. Ibraheem, and M. El-Azab Farid, Int. J. Mod. Phys. E **24**, 1550003 (2015).

[24] - M. A. Hassanain, Eur. Phys. J. A **52**, 8 (2016).

[25] - M. E. A. Farid and A. A. Ebrahim, Phys. Scr. **90**, 15301 (2015).

[26] - Y. X. Yang and Q. R. Li, Phys. Rev. C - Nucl. Phys. **72**, 1 (2005).

[27] - M. E.-A. Farid, Phys. Rev. C **65**, 67303 (2002).

[28] - J. C. Pacheco and J. A. Ruiz, **588**, 537 (1995).

[29] - N. Physics, N. P. Company, and A. Baeza, **437**, 93 (1985).

[30] - B. Bilwes, R. Bilwes, J. Díaz, J. L. Ferrero, J. C. Pacheco, and J. A. Ruiz, Nucl. Physics, Sect. A **484**, 174 (1988).

[31] - A. Baeza, J. Díaz, J. L. Ferrero, B. Bilwes, R. Bilwes, and J. Raynal, Phys. Lett. B **149**, 73 (1984).

[32] - B. Bilwes, R. Bilwes, J. Díaz, J. L. Ferrero, D. Počanić, and L. Stuttgé, Nucl. Phys. A **463**, 731 (1987).

[33] - B. Bilwes, R. Bilwes, J. Diaz, J. L. Ferrero, J. C. Pacheco, and J. A. Ruiz, Nucl. Phys. A **484**, 174 (1988).

[34] - M. A. Hassanain, M. Anwar, and K. O. Behairy, Phys. Rev. C **97**, (2018).

[35] - H. De Vries, C. W. De Jager, and C. De Vries, At. Data Nucl. Data Tables **36**, 495 (1987).

[36] - B. Energies and C. D. R. Nucldaires, **463**, 731 (1987).

[37] - B. Bilwes, R. Bilwes, L. Stuttge, F. Ballester, J. Diaz, J. L. Ferrero, C. Roldan, F. Sanchez, U. L. Pasteur, J. Diaz, J. L. Ferrero, C. Roldan, F. Sanchez, and D. F. Corpuscular, Nucl. Phys. A **473**, 353 (1987).

[38] - Z. M. M. Mahmoud, K. O. Behairy, A. A. Ibraheem, S. R. Mokhtar, M. A. Hassanain, and M. El-Azab Farid, J. Phys. Soc. Japan **88**, 1 (2019).

[39] - A. Hemmdan, F. O. M. Al Mahmody, and M. A. Hassanain, J. Phys. Soc. Japan **90**, 94201 (2021).

[40] - G. R. Satchler, *Direct Nuclear Reactions* (1983).

[41] - B. Pritychenko, M. Birch, B. Singh, and M. Horoi, At. Data Nucl. Data Tables **107**, 1 (2016).

[42] - D. Carbone, R. Linares, P. Amador-Valenzuela, S. Calabrese, F. Cappuzzello, M. Cavallaro, S. Firat, M. Fisichella, A. Spatafora, L. Acosta, C. Agodi, I. Boztosun, G. A. Brischetto, D. Calvo, E. R. Chávez Lomelí, I. Ciraldo, M. Cutuli, F. Delaunay, N. Deshmukh, P. Finocchiaro, A. Foti, A. Hacisalihoglu, F. Iazzi, L. La Fauci, G. Lanzalone, N. H. Medina, D. Mendes, J. R. B. Oliveira, A. Pakou, L. Pandola, H. Petrascu, F. Pinna, G. Russo, O. Sgouros, S. O. Solakci, V. Soukeras, G. Souliotis, D. Torresi, S. Tudisco, A. Yildirim, and V. A. B. Zagatto, Universe **7**, (2021).

[43] - J. Cook, Comput. Phys. Commun. **31**, 363 (1984).

[44] - I. J. Thompson, Comput. Phys. Reports **7**, 167 (1988).

[45] - L. Jarczyk, J. Okołowicz, A. Strzałkowski, K. Bodek, M. Hugi, L. Lang, R. Müller, and E. Ungricht, Nucl. Phys. A **316**, 139 (1979).